FINITE ELEMENT MODEL FOR NONLINEAR ANALYSIS OF FUNCTIONALLY GRADED PLATE/SHELL STRUCTURES

José Moita

jmoita50@gmail.com

FANOR, Faculdade Nordeste

Av. Santos Dumont, 7800, Fortaleza, Brasil.

LAETA, IDMEC, Instituto Superior Técnico, Universidade de Lisboa

Av. Rovisco Pais, 1049-001 Lisboa, Portugal

Aurélio Araújo

Cristóvão Mota Soares

aurelio.araujo@ist.utl.pt

cristovao.mota.soares@ist.utl.pt

LAETA, IDMEC, Instituto Superior Técnico, Universidade de Lisboa

Av. Rovisco Pais, 1049-001 Lisboa, Portugal

José Herskovits

jose@optimize.ufrj.br

COPPE-UFRJ, Universidade Federal do Rio de Janeiro

Ilha do Fundão, Rio de Janeiro, Brasil.

Abstract. *A finite element model applied for linear buckling and geometric nonlinear behavior analysis of general FGM plate-shell type structures is presented. Using the Newton-Raphson incremental-iterative method in conjugation with the updated Lagrangian formulation, the incremental equilibrium path is obtained, and in case of snap-through occurrence the automatic arc-length method is considered. The finite element is a non-conforming triangular flat plate/shell element with 24 degrees of freedom for the generalized displacements. The solutions of some illustrative plate/shell examples are presented and compared with numerical alternative models.*

Keywords: Nonlinear Analysis, FGM materials, plate-shell structures.

1 INTRODUCTION

The concept of functionally graded material (FGM) was first proposed by Koizumi (1993), in an effort to develop the super heat resistant materials. Typical FGM plate-shell type structures are made of Functionally Graded Materials whose are characterized by a continuous variation of the material properties over the thickness direction by mixing two different materials, metal and ceramic. The metal–ceramic FGM plates and shells are widely used in aircraft, space vehicles, reactor vessels, and other engineering applications.

In contrast with structures made of composite materials, in FGM plate-shell structures the smooth and continuous variation of the properties from one surface to the other eliminates abrupt changes in the stress and displacement distributions.

Geometric nonlinearity plays a significant role in the behavior of a plate or shells, especially when it undergoes large deformations. However a review of the literature shows that few studies have been carried out in nonlinear bending response of FGM plates and shells structures. This is the main reason to the present work, which include the nonlinear behavior and the linear buckling responses of this type of structures. Research in FGM structures has been done in the recent years. Among others, here we cite the following works: Praveen and Reddy (1998) carried out a nonlinear thermoelastic analysis of functionally graded ceramic–metal plates using a finite element model based on the first-order shear deformation theory (FSDT). Woo and Meguid (2001) provided an analytical solution for large deflection of FGM plates and shells under mechanical and thermal loading. Reddy and Arciniega (2007) carried out the large deformation analysis of FGM shells. Shariat and Eslami (2007) presented a closed-form solution for the critical buckling load of rectangular thick functionally graded plates under mechanical and thermal loads using the third order shear deformation plate theory. Kim et al. (2008) presented the geometric non-linear analysis of functionally graded material plates and shells using a four-node quasi-conforming shell element. Zhao and Liew (2009) analyzed the nonlinear response of functionally graded ceramic–metal shell panels under mechanical and thermal loading, using a displacement field expressed in terms of a set of mesh- free kernel particle functions. Zhao and Liew (2010), employed the first-order shear deformation plate theory, in conjunction with the element-free kp-Ritz method for the analysis of mechanical and thermal buckling of functionally graded ceramic–metal plates. Barbosa and Ferreira (2010) performed the geometric nonlinear analysis of functionally graded (FGM) plates and shells, using the Marguerre shell element. Huang et al. (2011) investigated the buckling behaviors of composite cylindrical shells made from functionally graded materials subjected to pure bending load. Results show that the inhomogenity of the materials is significant for buckling of FGM cylindrical shells. Ramu and Mohanty (2014) applied the finite element method, using the classical plate theory, for the modelling and buckling analysis of FGM rectangular plates, under uniaxial and biaxial compression loads along with simply supported boundary conditions.

In this paper, a large deformation analysis for functionally graded plate-shell structures is presented. The formulation includes geometric nonlinearity and linear buckling, and is implemented in a finite element model based on a non-conforming triangular flat plate/shell finite element in conjugation with the Reddy's third-order shear deformation theory.

2 FORMULATION OF FGM MODEL

An FGM is made by mixing two distinct isotropic material phases, for example a ceramic and a metal. The material properties of an FGM plate/shell structures are assumed to change continuously throughout the thickness, according to the volume fraction of the constituent materials. Power-law function (Bao and Wang, 1995) and exponential function (Delale and Erdogan, 1983) are commonly used to describe the variations of material properties of FGM. However, in both power-law and exponential functions, the stress concentrations appear in one of the interfaces in which the material is continuously but rapidly changing. Therefore, Chung and Chi (2001) proposed a sigmoid FGM, which was composed of two power-law functions to define a new volume fraction. They indicated that the use of a sigmoid FGM can significantly reduce the stress intensity factors of a cracked body.

To describe the volume fractions, the power-law function, and sigmoid function are used here. Thus, in this work, two models for estimating the effective material properties of the FGM at a point, are considered.

2.1 Power-Law function (P-FGM)

The volume fraction of the ceramic phase is defined according to the power-law:

$$V_c(z) = \left(0.5 + \frac{z}{h}\right)^p \tag{1}$$

being $z \in (-h/2;\ h/2)$, h the thickness of structure, and the exponent p a parameter that defines gradation of material properties across the thickness direction.

Thus, the metal volume fraction is

$$V_m(z) = 1.0 - V_c^k \tag{2}$$

2.2 Sigmoid function (S-FGM)

The volume fraction uses two power-law functions which ensure smooth distribution of stresses:

$$V_c(z) = 1.0 - \frac{1}{2}\left(\frac{h/2 - z}{h/2}\right)^p \qquad \text{for} \quad 0 \le z \le \frac{h}{2} \tag{3}$$

$$V_m(z) = \frac{1}{2}\left(\frac{h/2 + z}{h/2}\right)^p \qquad \text{for} \quad -\frac{h}{2} \le z \le 0 \tag{4}$$

In the present work, the continuous variation of the materials mixture is approximated by the using a certain number of layers throughout the thickness direction - layer approach. In this sense, the previous equations can be written for each layer as follows (considering the power-law function for example):

$$V_c^k = \left(0.5 + \frac{\bar{z}}{h}\right)^p \quad ; \quad V_m^k = 1.0 - V_c^k \tag{5}$$

where $\bar{z}$ is the thickness coordinate of mid-surface of each layer

Once the volume fraction V_c^k and V_m^k have been defined, the material properties (P) of each layer of an FGM can be determined by the rule of mixtures.

$$P^k = V_c^k P_c + V_m^k P_m \tag{6}$$

where P stands for Young's modulus E, the Poisson's ratio υ, the mass density ρ, or any other mechanical property.

Figure 1 show the variation of Young's modulus E through the thickness, obtained using the sigmoid function, and a 20 layer approach.

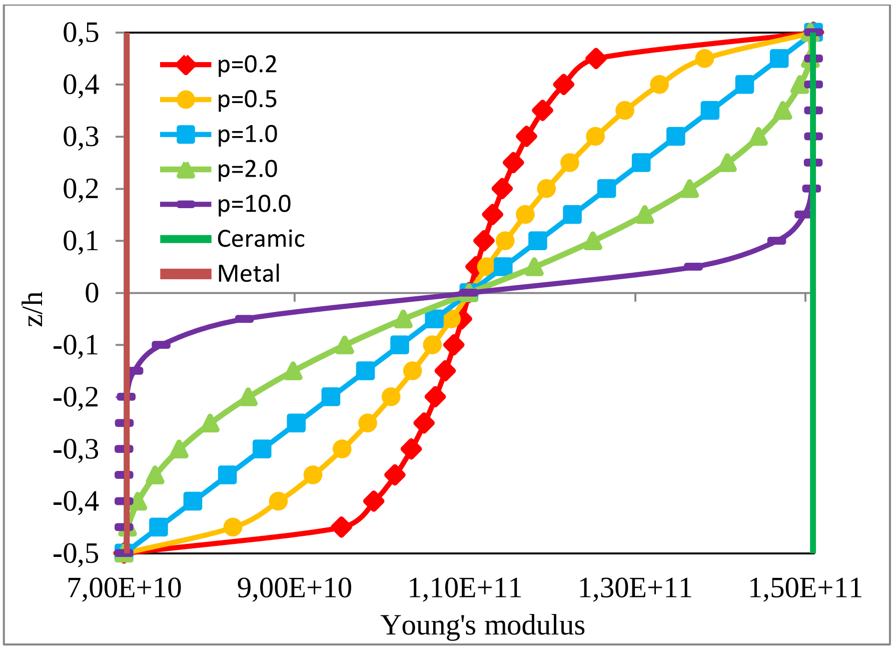

Figure 1. Variation of Young's modulus through the thickness.

3. NONLINEAR ANALYSIS THEORY.

3.1 Displacement field and strains

The objective of this work is to investigate the geometrically non-linear behavior of FGM plate/shell type structures under mechanical loading. The present theory considers large displacements with small strains. The used displacement field is based on the Reddy's third-order shear deformation theory, (Reddy, 2004):

$$u(x,y,z) = u_0^c(x,y) - z\,\theta_y(x,y) + z^3\,c_1\left[\theta_y(x,y) - \frac{\partial w_0}{\partial x}\right]$$

$$v(x,y,z) = v_0^c(x,y) + z\,\theta_x(x,y) + z^3\,c_1\left[-\theta_x(x,y) - \frac{\partial w_0}{\partial y}\right]$$
$$w(x,y,z) = w_0(x,y) \tag{7}$$

where u_0^c, v_0^c, w_0 are displacements of a generic point in the middle plane of the core layer referred to the local axes - *x,y,z* directions, θ_x, θ_y are the rotations of the normal to the middle plane, about the *x* axis (clockwise) and *y* axis (anticlockwise), $\partial w_0/\partial x$, $\partial w_0/\partial y$ are the slopes of the tangents of the deformed mid-surface in *x,y* directions, and $c_1 = 4/3h^2$, with h denoting the total thickness of the structure.

To the geometrically nonlinear behavior, the Green's strain tensor is considered. Its components are conveniently represented in terms of the linear and non-linear parts of the strain tensor as

$$\varepsilon = \left\{\varepsilon^L + \varepsilon^{NL}\right\} \tag{8}$$

The linear strain components associated with the displacement field defined above, can be represented in a synthetic form as:

$$\varepsilon^L = \begin{Bmatrix} \varepsilon_m + z\ \varepsilon_b + z^3\ \varepsilon_b^* \\ \varepsilon_s + z^2\ \varepsilon_s^* \end{Bmatrix} \tag{9}$$

and in de developed form as:

$$\varepsilon_{xx} = \frac{\partial u_0}{\partial x} - z\frac{\partial \theta_y}{\partial x} + z^3 c_1\left(\frac{\partial \theta_y}{\partial x} - \frac{\partial^2 w_0}{\partial x^2}\right)$$

$$\varepsilon_{yy} = \frac{\partial v_0}{\partial y} + z\frac{\partial \theta_x}{\partial y} + z^3 c_1\left(-\frac{\partial \theta_x}{\partial y} - \frac{\partial^2 w_0}{\partial y^2}\right)$$

$$\gamma_{xy} = \left(\frac{\partial u_0}{\partial y} + \frac{\partial v_0}{\partial x}\right) + z\left(-\frac{\partial \theta_y}{\partial y} + \frac{\partial \theta_x}{\partial x}\right) + z^3 c_1\left(\frac{\partial \theta_y}{\partial y} - \frac{\partial \theta_x}{\partial x} - 2\frac{\partial^2 w_0}{\partial x\,\partial y}\right)$$

$$\gamma_{xz} = -\theta_y + \frac{\partial w_0}{\partial x} + z^2 c_2\left(\theta_y - \frac{\partial w_0}{\partial x}\right)$$

$$\gamma_{yz} = \theta_x + \frac{\partial w_0}{\partial y} + z^2 c_2\left(-\theta_x - \frac{\partial w_0}{\partial y}\right) \tag{10}$$

where $c_2 = 4/h^2$.

The nonlinear strain components are given by

$$\varepsilon_{xx}^{NL} = \frac{1}{2}\left[\left(\frac{\partial u}{\partial x}\right)^2 + \left(\frac{\partial v}{\partial x}\right)^2 + \left(\frac{\partial w}{\partial x}\right)^2\right]$$

$$\varepsilon_{yy}^{NL} = \frac{1}{2}\left[\left(\frac{\partial u}{\partial y}\right)^2 + \left(\frac{\partial v}{\partial y}\right)^2 + \left(\frac{\partial w}{\partial y}\right)^2\right]$$

$$\gamma_{xy}^{NL} = \left[\left(\frac{\partial u}{\partial x}\frac{\partial u}{\partial y}\right) + \left(\frac{\partial v}{\partial x}\frac{\partial v}{\partial y}\right) + \left(\frac{\partial w}{\partial x}\frac{\partial w}{\partial y}\right)\right]$$

$$\gamma_{xz}^{NL} = \left[\left(\frac{\partial u}{\partial x}\frac{\partial u}{\partial z}\right) + \left(\frac{\partial v}{\partial x}\frac{\partial v}{\partial z}\right) + \left(\frac{\partial w}{\partial x}\frac{\partial w}{\partial z}\right)\right]$$

$$\gamma_{yz}^{NL} = \left[\left(\frac{\partial u}{\partial y}\frac{\partial u}{\partial z}\right) + \left(\frac{\partial v}{\partial y}\frac{\partial v}{\partial z}\right) + \left(\frac{\partial w}{\partial y}\frac{\partial w}{\partial z}\right)\right] \tag{11}$$

From the equations of displacement fields, for instance, the component ε_{xx}^{NL} is given by

$$\varepsilon_{xx}^{NL} = \frac{1}{2}\left[\frac{\partial u_0}{\partial x} - z\frac{\partial \theta_y}{\partial x} + z^3 c_1\left(\frac{\partial \theta_y}{\partial x} - \frac{\partial^2 w_0}{\partial x^2}\right)\right]^2 + \frac{1}{2}\left[\frac{\partial v_0}{\partial x} - z\frac{\partial \theta_x}{\partial x} + z^3 c_1 \left(-\frac{\partial \theta_x}{\partial x} - \frac{\partial^2 w_0}{\partial x \partial y}\right)\right]^2 + \frac{1}{2}\left(\frac{\partial w_0}{\partial x}\right)^2 \tag{12}$$

3.2 Constitutive Relations of FGM Structures

The constitutive equations for each layer k, can be written as follows:

$$\boldsymbol{\sigma}_k = \mathbf{Q}_k \; \boldsymbol{\varepsilon}_k \tag{13}$$

where $\boldsymbol{\sigma}_k = \{\sigma_x \;\; \sigma_y \;\; \sigma_{xy} \;\; \tau_{xz} \;\; \tau_{yz}\}^T$ is the stress vector and $\boldsymbol{\varepsilon}_k = \{\varepsilon_x \;\; \varepsilon_y \;\; \gamma_{xy} \;\; \gamma_{xz} \;\; \gamma_{yz}\}^T$ is the strain vector, $\mathbf{Q}_k$ is the elasticity matrix, whose non-zero elements are given by:

$$Q_{11} = Q_{22} = \frac{E^k}{1-\left(\nu^k\right)^2}\,; Q_{12} = Q_{21} = \nu^k \, Q_{11}\,; Q_{44} = Q_{55} = Q_{66} = \frac{E^k}{2\,(1+\nu^k)} = G^k \tag{14}$$

For each layer, the constitutive linear elastic relation is given as in (Moita et al., 2000):

$$\begin{Bmatrix} N \\ M \\ M^* \\ Q \\ Q^* \end{Bmatrix}_k = \begin{bmatrix} A & B & D & 0 & 0 \\ B & C & E & 0 & 0 \\ D & E & G & 0 & 0 \\ 0 & 0 & 0 & A_s & C_s \\ 0 & 0 & 0 & C_s & E_s \end{bmatrix}_k \begin{Bmatrix} \varepsilon_m \\ \varepsilon_b \\ \varepsilon_b^* \\ \varepsilon_s \\ \varepsilon_s^* \end{Bmatrix}_k \tag{15}$$

$$\hat{\boldsymbol{\sigma}}_k = \mathbf{D}_k \ \boldsymbol{\varepsilon}_k \tag{16}$$

4. VIRTUAL WORK PRINCIPLE. FINITE ELEMENT FORMULATION

The governing equations of the problem are obtained from the principle of virtual work in conjugation with an updated Lagrangian formulation (Bathe,1982). A reference configuration is associated with time t and the actualized configuration is associated with the current time $t' = t + \Delta t$. Thus we have:

$$\int_{{}^tV} {}^{t+\Delta t}_{\ \ t}S_{ij}\ \delta\ {}^{t+\Delta t}_{\ \ t}\varepsilon_{ij}\ d\ {}^tV = {}^{t+\Delta t}_{\ \ t}\Re \tag{17}$$

where the first and second member are the internal and external virtual work, respectively, and ε_{ij} and S_{ij} are the Green-Lagrange strain components and the second Piola-Kirchhoff stress components respectively.

Taking the Virtual Work Principle equation and doing the incremental decomposition of the stress and strain tensors, we obtain a new equation in a incremental form.

$$\int_{{}^tV} {}_tS_{ij}\ \delta\ {}_t\varepsilon_{ij}\ d\ {}^tV + \int_{{}^tV} {}^t\tau_{ij}\ \delta\ {}_t\eta_{ij}\ d\ {}^tV = {}^{t+\Delta t}_{\ \ t}\Re - \int_{{}^tV} {}^t\tau_{ij}\ \delta\ {}_te_{ij}\ d\ {}^tV \tag{18}$$

where ${}^t\tau_{ij}$ are the incremental components of the Cauchy stress tensor, ${}_te_{ij}$ are the incremental components of the linear strain vector, and ${}_t\eta_{ij}$ are the incremental components of the nonlinear strain vector.

In the present works it is used a non-conforming triangular plate/shell finite element model having three nodes and eight degrees of freedom per node: the displacements u_{0_i}, v_{0_i}, w_{0_i}, the slopes $(-\partial w_0/\partial y)_i$, $(\partial w_0/\partial x)_i$ and the rotations $\theta_{xi}, \theta_{yi}, \theta_{zi}$. The rotation θ_{zi} is introduced to consider a fictitious stiffness coefficient $K_{\theta Z}$ to eliminate the problem of a singular stiffness matrix for general shape structures (Zienkiewicz, 1977). The element local displacements, rotations and slopes, are expressed in terms of nodal variables through shape functions ${}_j\mathbf{N}_i$ given in terms of area co-ordinates L_i. The displacement field can be represented in matrix form as:

$$\mathbf{u} = \mathbf{Z}\left(\sum_{i=1}^{3}\mathbf{N}_i\ \mathbf{d}_i\right) = \mathbf{Z}\,\mathbf{N}\,\mathbf{a} \quad ; \quad \mathbf{d} = \sum_{i=1}^{3}\mathbf{N}_i\ \mathbf{d}_i = \mathbf{N}\,\mathbf{a} \tag{19}$$

where the appropriate matrix $\mathbf{Z}$ containing powers of z_k, and the element and nodal displacement vectors, $\mathbf{a}$ and $\mathbf{d}_i$ respectively, are given in (Moita et al., 2000).

The membrane, bending and shear strains, as well the higher order bending and shear strains can be represented by:

$$\boldsymbol{\varepsilon}_m = \mathbf{B}^m \mathbf{a} \; ; \; \boldsymbol{\varepsilon}_b = \mathbf{B}^b \mathbf{a} \; ; \; \boldsymbol{\varepsilon}_s = \mathbf{B}^s \mathbf{a} \; ; \; \boldsymbol{\varepsilon}_b^* = \mathbf{B}^{*b} \mathbf{a} \; ; \; \boldsymbol{\varepsilon}_s^* = \mathbf{B}^{*s} \mathbf{a} \tag{20}$$

where the $\mathbf{B}^m$, $\mathbf{B}^b$, $\mathbf{B}^{*b}$, $\mathbf{B}^s$, $\mathbf{B}^{*s}$, are components of the strain-displacement matrix $\mathbf{B}$, and are given explicitly in Moita et al. (2011).

The Virtual Work Principle equation (18) applied to a finite element can be written in the form:

$$\begin{aligned}
&\sum_{k=1}^{N}\left\{ \int_{{}^tA^e} \int_{h_{k-1}}^{k_k} \delta\left({}_t\varepsilon_k^L\right) Q_k \; {}_t\varepsilon_k^L \, dz \; {}^t dA^e + \int_{{}^tA^e} \int_{h_{k-1}}^{k_k} \delta\left({}_t\varepsilon_k^{NL}\right) {}^t\sigma_k^L \, dz \; {}^t dA^e \right\} = \\
&{}_t^{t+\Delta t}\Re^e - \sum_{k=1}^{N} \int_{{}^tA^e} \int_{h_{k-1}}^{k_k} \delta\left({}_t\varepsilon_k^L\right) {}^t\sigma_k^L \, dz \; {}^t dA^e
\end{aligned} \tag{21}$$

From this equation we obtain the element linear stiffness matrix $\mathbf{K}_L^e$, as well as the the element external load vector $\mathbf{F}_{ext}^e$ and the element internal force vector $\mathbf{F}_{int}^e$, and their definition are explicitly given in Moita et al. (2011). The element geometric stiffness matrix $\mathbf{K}_\sigma^e$, is obtained with a fully development, in the same way as shown in (Moita et al.,1996).

Those matrices and vectors are initially computed in the local coordinate system attached to the element. To solve general structures, local - global transformations are needed. Doing these transformations, and after adding the contributions of all the elements in the domain, the following system of equilibrium equations is obtained for geometrically nonlinear analysis:

$${}_{t+\Delta t}^{t+\Delta t}\left(\mathbf{K}_L + \mathbf{K}_\sigma\right)^{i-1} \left(\Delta\mathbf{q}\right)^i = {}^{t+\Delta t}\mathbf{F}_{ext} - {}_{t+\Delta t}^{t+\Delta t}\left(\mathbf{F}_{int}\right)^{i-1} \tag{22}$$

Using the Newton-Raphson incremental-iterative method (Bathe and Ho, 1981), the incremental equilibrium path is obtained, and in case of snap-through occurrence the automatic arc-length method is used (Crisfield, 1980) and (Moita et al., 2000). Equation (22) is then written in the form:

$${}_{t+\Delta t}^{t+\Delta t}\left(\mathbf{K}_L + \mathbf{K}_\sigma\right)^{i-1} \left(\Delta\mathbf{q}\right)^i = \left(\lambda^{i-1} + \Delta\lambda^i\right)\mathbf{F}_{ext}^0 - {}_{t+\Delta t}^{t+\Delta t}\left(\mathbf{F}_{int}\right)^{i-1} \tag{23}$$

and an additional equation is employed to constrain the length of a load step:

$$\left(\Delta\mathbf{q}\right)^{i^T}\left(\Delta\mathbf{q}\right)^i = \left(\Delta l\right)^2 \tag{24}$$

where $\mathbf{F}_{\text{ext}}^{0}$ is a fixed (reference) load vector, λ is a load factor, $\Delta\lambda$ is the incremental load factor within the load step, and Δl is the arc-length.

For linear buckling analysis, we make use of only one load increment, and equation (21) takes the following form:

$$(\mathbf{K}_{\text{L}} + \mathbf{K}_{\sigma})\mathbf{q} = \mathbf{F}_{\text{ext}} \tag{25}$$

The instability takes place when the determinant of the tangential matrix is zero. It occurs for a certain value of geometric stiffness matrix defined by

$${}^{cr}\mathbf{K}_{\text{L}} = \lambda_{cr}\,\mathbf{K}_{\sigma} \tag{26}$$

Thus, we have

$$\det(\mathbf{K}_{\text{L}} + \lambda_{cr}\,\mathbf{K}_{\sigma}) = 0 \tag{27}$$

and the corresponding eigenvalue problem is solved, obtaining the critical load as follows

$$(\mathbf{K}_{\text{L}} + \lambda_{cr}\,\mathbf{K}_{\sigma})\mathbf{q} = 0 \tag{28}$$

$${}^{cr}\mathbf{F}_{\text{ext}} = \lambda_{cr}\,\mathbf{F}_{\text{ext}} \tag{29}$$

where in the Eq. (22-29), $\mathbf{K}_{\text{L}}$, $\mathbf{K}_{\sigma}$, $\mathbf{F}_{\text{ext}}$, $\mathbf{F}_{\text{int}}$, $\Delta\mathbf{q}$, and $\mathbf{q}$ are the system stiffness matrix, geometric stiffness matrix, external load vector, internal load vector, incremental displacement vector and displacement vector, in global coordinate system, respectively

5. NUMERICAL APPLICATIONS

5.1 Simply supported square S- FGM plate. Linear analysis.

A simply supported square (axa) plate under uniformly distributed load of intensity $q_0 = 1.0\,\text{N/m}^2$, presented by Kim et al. (2008), is analyzed using the present model. The mechanical properties of the isotropic ceramic material are E_c = 151 x 10^9 N/m^2, ν_c = 0.3 and for isotropic metal material are E_m = 70 x10^9 N/m^2, ν_m = 0.30. The side to thickness ratio is a/h=100. The S-FGM plate is modeled by using different finite element meshes from 8x8 (128 triangular elements) to 24x24 (1152 triangular elements). In this application and all the the FGM cases, the layered approach was carried out with 10 layers. This value had been chosen based on a convergence study.

The non-dimensional center deflections $w^* = w\left(E_c\,h^3/q_0\,a^4\right)$ are shown in Table 1. From this table it can be observed that the result given by the present finite element FGM model using a 24x24 element mesh have an excellent agreement with the result obtained by the Navier analytical solution (Kim et al., 2008).

For the same application, the Figure 2 shows the center deflection as a function of the power-law index. The discrepancies between the results of present model and the analytical solution are about of 0.4%. Also is observed that under the same load, the case of p=10 has the largest center deflection. This is due to the fact that it has the lowest Young's modulus.

Table 1. Normalized center deflection of S-FGM plate (index p=10).

Mesh	Normalized deflection	Error %
8x8	0.06209	7.6
12x12	0.06572	2.2
16x16	0.06660	0.9
20x20	0.06680	0.6
24x24	0.06699	0.3

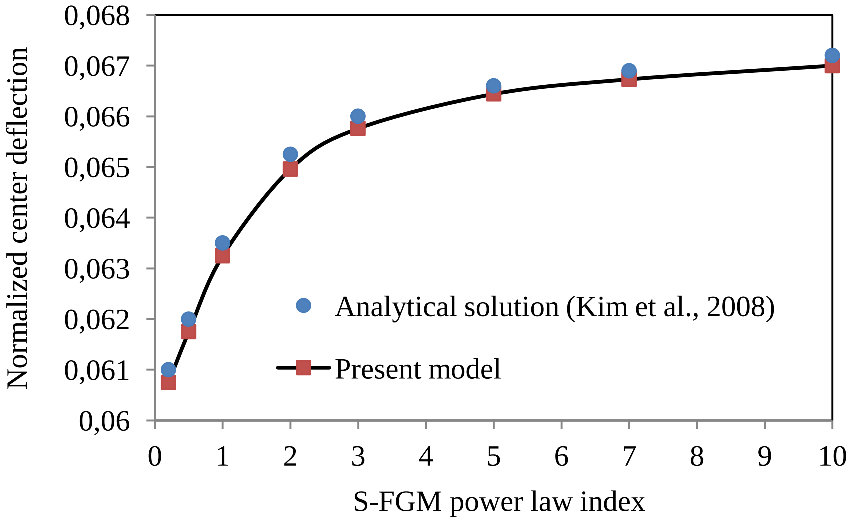

Figure 2. Center deflection versus power law index

5.2 Geometrically nonlinear analysis of a functionally graded plate strip

A cantilevered FGM plate strip subjected to a bending distributed moment on the other end is considered. The material properties for the ceramic and metal constituents are E_c = 151 x 10^9 N/m^2, $\nu_c = 0.3$, E_m = 70 x10^9 N/m^2, $\nu_m = 0.30$. The geometry of the plate is L =12.0 m, b = 1.0 m, h = 0.1 m. The total bending moment M_{Ref} = 65, 886.17926 N.m.

Figure 3 show the results for the tip deflection due to a bending distributed moment M for the different power-law p-index considered, obtained by the present model - (P M). In the same figure are presented the results obtained by Arciniega and Reddy (2007) - (A & R) , and is observed a good agreement between both solutions. In Figure 4 are shown the deformed shapes of the plate strip for specific load levels.

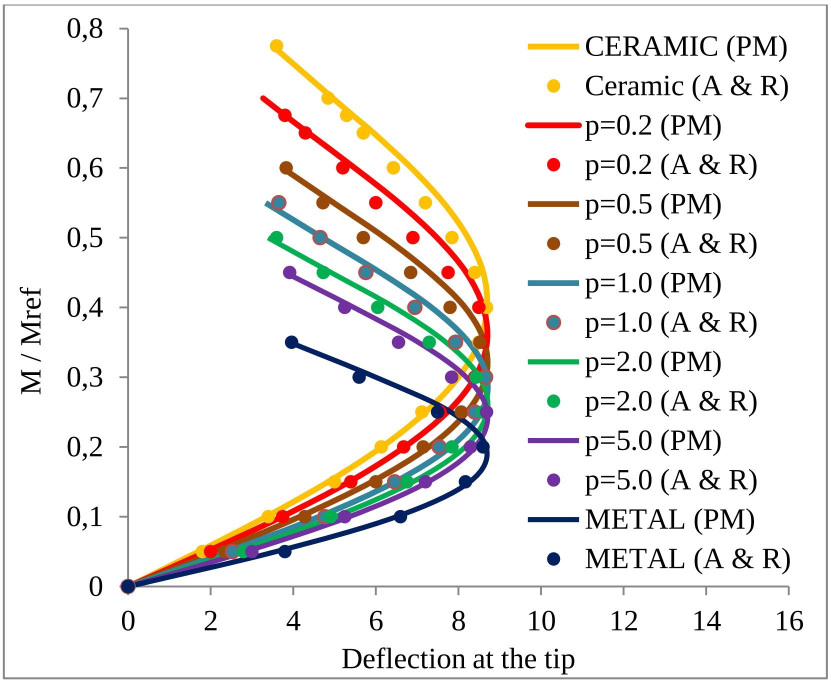

Figure 3. Tip-deflection W versus end moment M for the FGM plate strip.

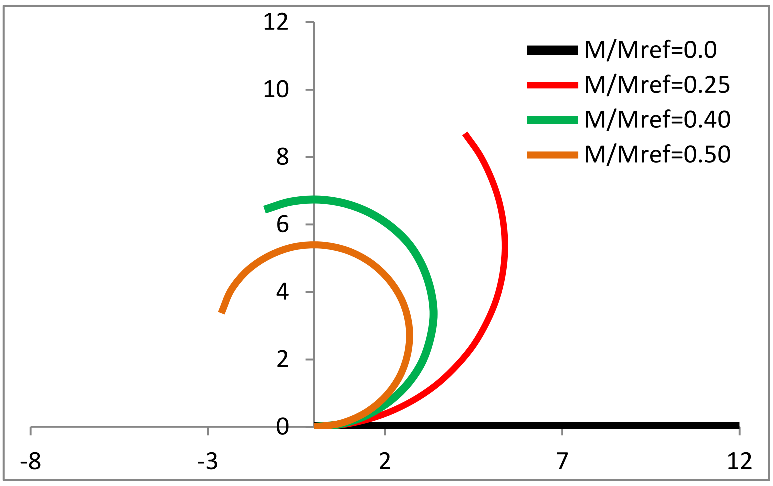

Figure 4. Initial and deformed shapes of plate strip

5.3 Geometrically nonlinear analysis of a clamped functionally graded cylindrical panel

A square clamped P-FGM cylindrical shell panel (Figure 5), with constituents zirconia and aluminum, which material properties are E_c = 151 x 10^9 N/m^2, ν_c = 0.3, E_m = 70 x10^9 N/m^2, ν_m = 0.30, with several power law exponents p is considered. The geometry of the panel is side L=0.2 m, radius R=1.0 m, thickness h=0.01 m, and θ=0.1 rad. The panel is modeled by a 16x16 finite element mesh (512 triangular elements). Figure 6 shows the non-dimensional center deflection w/h due to the non-dimensional load parameter $p = P_0 L^4 / E_m h^4$ of a uniform radial pressure load, for the different power-law p-index considered. The results obtained with the present model have a good agreement with those obtained by Zhao and Liew (2009) and as expected, the case of pure metal has the largest center deflection, and the case of pure ceramic has the smallest center deflection. Also is observed that the deflection curves of the functionally graded material panels are located between those of the metal and ceramic panels.

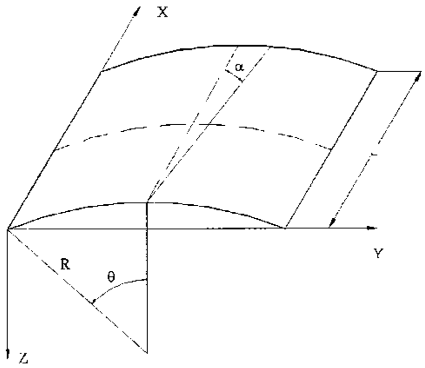

Figure 5. Cylindrical panel.

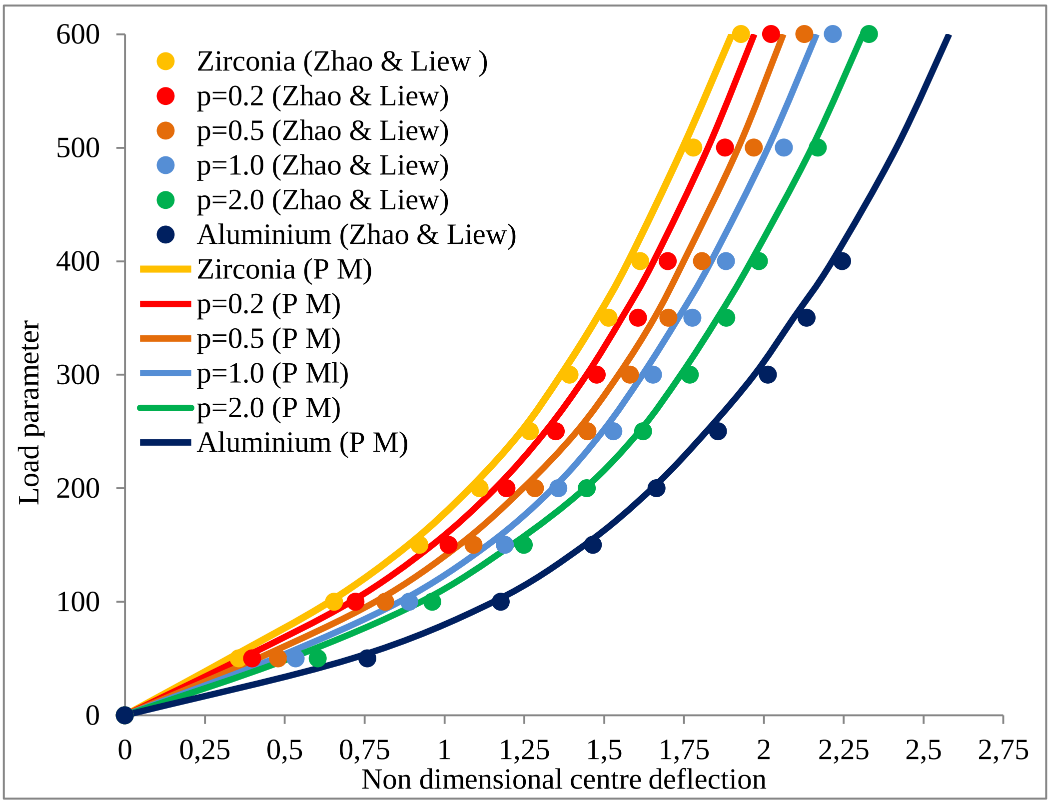

Figure 6. Load-deflection curves for different power law index

5.4 Rectangular P-FGM plates under uniaxial and biaxial compression

The buckling analysis of a rectangular (axb) P-FGM plate made of a mixture of silicon nitride and stainless steel is considered. The material properties for the silicon nitride and stainless steel are E_c = 322.27 x 10^9 N/m^2, $\nu_c = 0.24$, E_m = 207.78 x10^9 N/m^2, $\nu_m = 0.3177$. The FGM plates of two different aspect ratios a/b, are under uniaxial compression over the side of length b=1 m, or biaxial compression, and the power law index takes different values: p= 0, 1, 2, 5.

Tables 2 and 3 show the critical buckling loads for FGM plates with aspect ratios a/b=0.25 and a/b=1 and different values for the ratio h/b. From the obtained results, a good agreement with those (R&M) obtained by Ramu and Mohanty (2014) is observed. Also the influence of the power-index and the ratio t/b, observed in the Tables are according with what would be predictable.

Table 2. The critical buckling load (MN/m) of FGM rectangular plates, under uniaxial compression

Aspect ratio	Power law Index	Uniaxial compression		
		h=0.01 m	h=0.02 m	h=0.03 m
a/b=0.25	0 (Present)	5.0672	39.890	131.52
	(R&M)	5.0576	40.461	136.56
	1 (Present)	4.2070	33.050	109.95
	(R&M)	4.3156	34.525	116.52
	2 (Present)	4.0223	31.622	104.11
	(R&M)	4.0470	32.376	109.27
	5 (Present)	3.8399	30.132	99.42
	(R&M)	3.7379	29.903	100.92
a/b=1.0	0 (Present)	1.1334	9.0147	30.216
	(R&M)	1.1222	8.9104	30.072
	1 (Present)	0.9416	7.4784	25.256
	(R&M)	0.9502	7.0618	25.656
	2 (Present)	0.9012	7.1610	24.086
	(R&M)	0.8910	7.1283	24.058
	5 (Present)	0.8536	6.8506	23.027
	(R&M)	0.8229	6.5834	22.219

4.5 P-FGM Cylindrical Panel Under Uniaxial Compressive Pressure

The buckling analysis of a square P-FGM plate made of a mixture of aluminum and zirconia with the following properties E_m = 70.0 x10^9 N/m^2, ν_m = 0.3, E_c = 151.0 x 10^9 N/m^2, ν_c = 0.3, is considered. The geometry of the panel is length L = 0.1m, span angle 2θ = 0.2 rad, radius R = 0.5 m, and thickness h = 0.001 m, The FGM panel is assumed to be with the curved edges fixed and the straight edges simply-supported (FSFS). The panel is under uniaxial compression applied on the curved edges. A 20x20 finite element mesh is used (800 triangular elements). The results for buckling load parameter $\overline{N}_{cr} = N_{cr} R / E_m h^2$ for the first four modes are given in Table 4 for the different power law index considered. From this Table a good agreement with the results obtained by Zhao and Liew (2010) is observed, with discrepancies varying from 1% to 10 %, This discrepancies may be due to the different models and solution strategies.

Table 3. The critical buckling load (MN/m) of FGM rectangular plates, under biaxial compression

Aspect ratio	Power law index		Biaxial compression		
			h=0.01 m	h=0.02 m	h=0.03 m
a/b=0.25	0	(Present)	4.9910	39.272	129.46
		(R&M)	4.7601	38.081	128.52
	1	(Present)	4.1356	32.528	107.17
		(R&M)	3.9373	31.499	106.31
	2	(Present)	3.9601	31.120	102.40
		(R&M)	3.7899	30.319	102.33
	5	(Present)	3.7912	29.767	97.792
		(R&M)	3.6517	29.214	98.597
a/b=1.0	0	(Present)	0.55673	4.5074	15.143
		(R&M)	0.55692	4.4552	15.036
	1	(Present)	0.47065	3.7442	12.578
		(R&M)	0.44605	3.6845	12.435
	2	(Present)	0.45080	3.5854	12.043
		(R&M)	0.44329	3.5463	11.969
	5	(Present)	0.43129	3.4303	11.519
		(R&M)	0.42712	3.4168	11.532

Table 4. The critical buckling load $\overline{N}_{cr}$ of a P-FGM cylindrical panel under uniaxial compression and FSFS boundary conditions

Model	Mode	p=0.0	p=0.5	p=1.0	p=2.0	p=5.0	p=10.0	p=20.0
Z&L	1	1.7195	1.3700	1.2229	1.1025	0.9949	0.9303	0.8783
PM		1.7574	1.3943	1.2355	1.1074	0.9970	0.9314	0.8761
Z&L	2	1.8416	1.4575	1.3001	1.1796	1.0750	1.0072	0.9489
PM		1.9526	1.5460	1.3727	1.2385	1.1237	1.0492	0.9818
Z&L	3	2.3913	1.8863	1.6837	1.4017	1.4018	1.3149	1.2374
PM		2.2338	1.7397	1.5354	1.3842	1.2665	1.1901	1.1185
Z&L	4	2.4746	1.9463	1.7373	1.4559	1.4559	1.3669	1.2853
PM		2.4630	1.9212	1.6963	1.5290	1.3986	1.3152	1.2351

6. CONCLUSIONS

A finite element model was formulated for the linear buckling and the static nonlinear analysis of functionally graded materials plates-shell structures. The model is based on the Reddy’s third order shear deformation theory, implemented in a non-conforming flat triangular plate/shell element with 24 degrees of freedom for the generalized displacements. The continuous variation of the mechanical properties through the thickness is approximated by only 10 layers for all applications, which preserves the reduced computational time of the present model. From the results obtained by the present model, in general, a very good accuracy is found between the present model and with alternative models.

ACKNOWLEDGEMENTS

This work was supported by FCT, Fundação para a Ciência e Tecnologia, through IDMEC, under LAETA, project UID/EMS/50022/2013, and also CNPq, CAPES and FAPERJ, from Brazil

REFERENCES

Arciniega R. A., Reddy, J. N., 2007. Large deformation analysis of functionally graded shells. *International Journal of Solids and Structures*, 44, pp. 2036–2052.

Bao, G. and Wang, L., 1995. Multiple Cracking in Functionally Graded Ceramic/Metal Coatings. *International Journal of Solids and Structures*, 32, pp. 2853–2871.

Barbosa A.T., and Ferreira A.J.M., 2010. Geometrically Nonlinear Analysis of Functionally Graded Plates and Shells. *Mechanics of Advanced Materials and Structures*, 17, pp. 40–48.

Bathe, K.J., 1982. *Finite Element Procedures in Engineering Analysis*, Prentice-Hall Inc, Englewood Cliffs, New Jersey.

Bathe K.J., Ho L.W., 1981. A simple and e• cient element for analysis of general shell structures. *Computers and Structures*, 13, pp. 673-681.

Chi, S.H. and Chung, Y.L., 2002. Cracking in Sigmoid Functionally Graded Coating. *Journal of Mechanics*, 18, pp. 41–53.

Chung, Y.L. and Chi, S.H., 2001. The Residual Stress of Functionally Graded Materials. *Journal of Chinese Institute of Civil and Hydraulic Engineering*, 13, pp. 1–9.

Delale, F. and Erdogan, F., 1983. The Crack Problem for a Nonhomogeneous Plane, ASME, *Journal of Applied Mechanics*, 50, pp. 609–614.

Crisfield, M.A., 1980. A fast incremental/iterative solution procedure that handles ´snap-through´. *Computers and Structures*, 62, pp. 13-55.

Huang, H., Han, Q., Wei, D., (2011). Buckling of FGM cylindrical shells subjected to pure bending load. *Composite Structures*, 93, pp. 2945–2952

Koizumi, M., 1993. The concept of FGM Ceramic. Trans. Funct. Grad. Mater. 34, pp. 3–10

Kim, K.D., Lomboy, G. R., & Han, S. C., 2008. Geometrically Non-linear Analysis of Functionally Graded Material (FGM) Plates and Shells using a Four-node Quasi-Conforming Shell Element, *Journal of Composite Materials*, 42, 5, pp. 485-511

Moita, J. S., Mota Soares, C. M., Mota Soares, C. A., 1996. Buckling behaviour of laminated composite structures using a discrete higher-order displacement model. *Composite Structures* 35, pp. 75-92.

Moita, J.S., Barbosa, J. I., Mota Soares, C. M., and Mota Soares, C. A., 2000. Sensitivity analysis and optimal design of geometric non-linear laminated plates and shells. *Computers and Structures*, 76, pp. 407-420.

Moita, J. S., Araújo, A. L., Martins, P.G., Mota Soares, C. M.,and Mota Soares, C.A., 2011. Analysis of active-passive plate structures using a simple and efficient finite element model. *Mechanics of Advanced Materials and Structures*, 18, pp. 159-169.

Praveen, G.N., Reddy, J.N., 1998. Nonlinear transient thermoelastic analysis of functionally graded ceramic–metal plates. *Int. J. Solids Struct.* 35, pp. 4457-4476.

Ramu, I, Mohanty, S. C., (2014). Buckling Analysis of Rectangular Functionally Graded Material Plates under Uniaxial and Biaxial Compression Load, *Procedia Engineering*, 86, pp. 748-757

Reddy, J.N., 2004. *Mechanics of Laminated Composite Plates and Shells*, 2 nd Edition. CRC Press.

Shariat B. A.S., Eslami, M. R., 2007. Buckling of thick functionally graded plates under mechanical and thermal loads, *Composite Structures*, 78, pp. 433–439

Woo, J., Meguid, S.A., 2001. Nonlinear analysis of functionally graded plates and shallow shells. *Int. J. Solids Struct.* 38, pp. 7409–7421.

Zhao, X., Liew, K. M., 2009. Geometrically nonlinear analysis of functionally graded shells. *International Journal of Mechanical Sciences*, 51, pp. 131–144

Zhao, X., Liew, K. M., 2010. A mesh-free method for analysis of the thermal and mechanical buckling of functionally graded cylindrical shell panels, *Comput. Mech.*, 45, pp. 297–310.

Zienkiewicz OC., 1977. *The fnite element method*. New York, USA: McGraw-Hill.